Nanostructures

Polyol Synthesis of Platinum Nanostructures: Control of Morphology through the Manipulation of Reduction Kinetics**

*Jingyi Chen, Thurston Herricks, and Younan Xia**

A great deal of effort has been directed towards the synthesis of nanostructures that have well-controlled morphology.[1] It is generally accepted that the morphology (including dimensionality and shape) of a nanostructure may allow tuning that is as powerful as tuning with size for tailoring the electronic, optical, magnetic, and catalytic properties of a functional material. Herein we report a case study in which the morphology of Pt nanostructures could be readily controlled by manipulating the reduction kinetics of a polyol synthesis. More specifically, Pt nanostructures in the form of spheres, star-shaped particles, branched multipods, and uniform nanowires have been successfully synthesized by coupling the polyol reduction of a platinum precursor with the Fe^{II}/Fe^{III} redox pair and the adsorption of oxygen and nitrogen gases.

Platinum plays an important role in many industrial applications.[2] For example, it serves as a catalyst in the reduction of pollutant gases emitted from automobiles, the synthesis of nitric acid, oil cracking, and proton-exchange membrane (PEM) fuel cells.[3] All of these applications require the use of Pt as fine particles. It has also been established that both the reactivity and selectivity of Pt nanostructures in a catalytic reaction are highly dependent on the morphology and therefore on the crystallographic planes exposed on the surface of the nanoparticles.[4]

For these reasons, much effort has been devoted to the production of Pt nanostructures with monodispersed sizes and well-defined morphologies. Most of these studies, however, have been limited to Pt nanoparticles that could be easily synthesized by using a variety of chemical methods.[5] In general, such a synthesis involves the reduction of a Pt^{IV} or Pt^{II} precursor in the presence of a polymeric stabilizer by using reducing agents such as alcohol, sodium borohydride, or hydrogen gas. While the resultant nanoparticles may be considered monodisperse in size, they are often spherical or lack well-defined facets. The formation of well-faceted nanoparticles has only been demonstrated in a limited number of examples in which hydrogen gas was used as the reducing agent and sodium polyacrylate as the stabilizer.[6] Another chemical method of generating faceted Pt nanoparticles is based on the reduction of a Pt^{IV} precursor with sodium borohydride in water at 0 °C, followed by phase transfer of the reduced species to an organic solvent.[7] The mechanism responsible for the formation of these faceted nanoparticles has yet to be elucidated. In a different approach, nanorods and nanotubes of polycrystalline Pt have been fabricated by templating against channels in porous materials,[8] as well as Ag or Se nanowires.[9] Kijima et al. have also demonstrated the synthesis of Pt nanotubes by employing self-assembled structures of surfactants as the template.[10] Although template-based syntheses have proven to be straightforward and versatile, they are restricted by a number of drawbacks that include the requirement of template removal to obtain a pure product, the limited scope of morphological variation, and the polycrystallinity often associated with the product.

In a recent study,[11] we discovered that the addition of a trace amount of iron species (Fe^{II} or Fe^{III}) to a polyol process could significantly alter the growth kinetics of Pt nanostructures and thus induce the formation of Pt nanowires. These nanowires are characterized by uniform diameters and relatively high aspect ratios. Herein we demonstrate that the reduction kinetics can be further manipulated to obtain several other morphologies such as branched multipods. On the basis of our results from UV/Vis and X-ray photoelectron spectroscopy (XPS), we believe that the reduction of a Pt^{IV} precursor with polyol proceeds through two steps and involves a Pt^{II} intermediate (Figure 1).

After the reaction had proceeded in air at 110 °C for 1.5 h, all of the Pt^{IV} precursor was converted into a Pt^{II} species. When cooled down to room temperature and stored in a vial

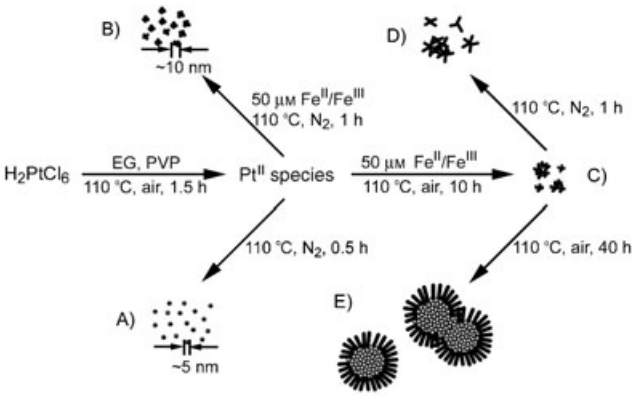

Figure 1. Four different ways to control the kinetics of polyol reduction and the corresponding morphologies observed for the Pt nanostructures. As the same amount of PVP was present in all four illustrated syntheses, the striking difference in morphology was not caused by PVP concentration. We believe that the PVP molecules in these syntheses only function as a stabilizer to prevent the resultant nanoparticles from aggregating into larger structures.

[*] J. Chen, T. Herricks, Prof. Y. Xia
Department of Chemistry
University of Washington
Seattle, WA 98195-1700 (USA)
Fax: (+1) 206-685-8665
E-mail: xia@chem.washington.edu

[**] This work has been supported in part by a DARPA–DURINT subcontract from Harvard University and a fellowship from the David and Lucile Packard Foundation. Y.X. is an Alfred P. Sloan Research Fellow and a Camille Dreyfus Teacher Scholar. J.C. and T.H. thank the Center for Nanotechnology at the University of Washington for a Nanotech Student Fellowship Award and an IGERT Fellowship Award (supported by the NSF, DGE-9987620), respectively. This work was performed in part at the Nanotech User Facility (NTUF), a member of the National Nanotechnology Infrastructure Network (NNIN) funded by the NSF.

Supporting information for this article is available on the WWW under http://www.angewandte.org or from the author.

 DOI: 10.1002/ange.200462668

under ambient conditions, the Pt^{II} intermediate could be left for more than one month without being further reduced to Pt^0. However, if the reaction was allowed to continue in air at 110 °C, the Pt^{II} species was fully reduced to produce spherical Pt nanoparticles of about 5-nm diameter within 1 h. In such a case, the reduction of the Pt^{II} species was greatly accelerated by an autocatalytic process once some Pt nuclei had formed in solution.[12] When this process was carried out under nitrogen atmosphere, the reduction of Pt^{II} species to Pt^0 became faster than in air, and spherical nanoparticles (Figure 1 A) were formed in the solution within 30 min. This observation implies that the adsorption of oxygen from air onto the surface of Pt nuclei was able to slow down the autocatalytic reduction of the Pt^{II} species.[13] Although the presence of oxygen could slow down this process, the reduction was still too fast to induce the formation of structures that deviated from the equilibrium shape.[14]

In contrast, the reduction of the Pt^{II} species could be retarded when an Fe^{II} or Fe^{III} species was introduced into the reaction mixture. In this case, Fe^{III} ions oxidized both Pt atoms and nuclei back to Pt^{II} species and thus significantly decreased the supersaturation of the Pt atoms (see Supporting Information). As the resultant Fe^{II} ions could be recycled back to Fe^{III} ions by aerial oxygen, only a small amount of Fe^{III} was needed in this synthesis. For the same reason, both Fe^{II} and Fe^{III} ions have the same function in controlling the reduction kinetics. The present work suggests that oxygen can slow down the growth through both surface adsorption and etching mechanisms when coupled with the Fe^{II}/Fe^{III} species. In general, it is hard to single out which mechanism is the dominant because both retardation effects have a strong dependence on the concentrations of oxygen and the Fe^{II}/Fe^{III} species. By taking advantage of these two mechanisms, the rate of reduction of the Pt^{II} species could be regulated; a range of products from A to E can be formed, with a slower reduction favoring the formation of E and a faster reduction favoring the formation of A. In general, as the reduction became slower, the growth of [111] planes increased, thus leading to the formation of highly anisotropic (branched and then 1D) nanostructures.

Figure 1 summarizes the major products that were observed when trace amounts of Fe^{II} or Fe^{III} species (with a final concentration of 50 μM) and/or nitrogen were introduced into the reaction system after the formation of the Pt^{II} species. Depending on whether the reaction was allowed to continue in air or under nitrogen, the Pt nanostructures were found to display different morphologies. Under a nitrogen atmosphere, star-shaped nanoparticles (Figure 1 B) were produced over a period of 1 h, while in air the reaction proceeded at a much slower rate and the nanostructures became more branched and subsequently assembled into submicrometer-sized agglomerates (Figure 1 C). Towards the end of this reaction, the Pt^{II} species were reduced at an extremely slow rate to generate uniform Pt nanowires (Figure 1 E) on the surface of each agglomerate. However, when nitrogen was applied, the reduction rate slightly increased and resulted in the formation of multipods with highly branched structures (Figure 1 D).

It is worth noting that the mechanism involved in the present work seems to be different from the model developed by Peng for CdSe nanostructures.[15] Highly anisotropic (branched and 1D) CdSe nanostructures were obtained at high monomer concentrations—and thus high reduction rates and supersaturations—and spherical CdSe nanoparticles were formed at low monomer concentrations.[15]. The trend that Peng observed for CdSe nanostructures is exactly the opposite of the trend we have observed as we found that highly anisotropic Pt nanostructures were only formed at extremely low supersaturations. If the reduction proceeded too quickly and hence the supersatuation was too high, only isotropic, spherical Pt nanoparticles were produced.

Figure 2 shows TEM and SEM images of the Pt nanostructures that correspond to the products illustrated in Figure 1. Consistent with the schematic drawing, the products

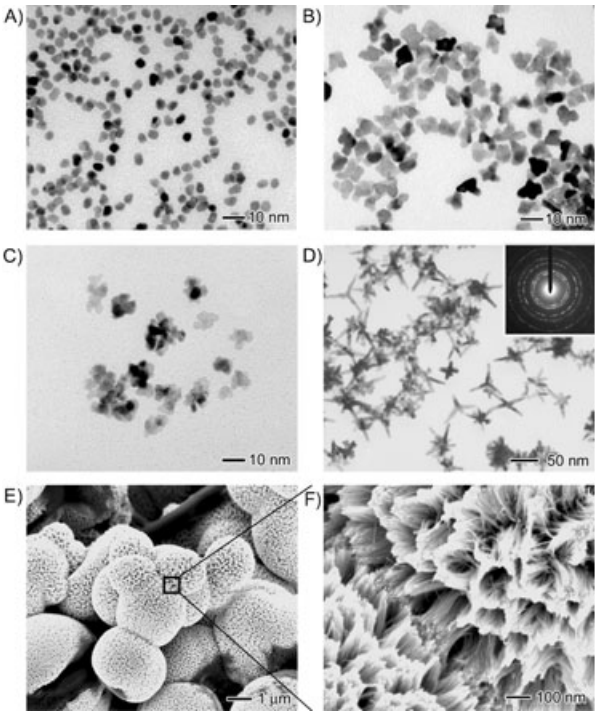

Figure 2. TEM (A–D) and SEM (E, F) images of Pt nanostructures that have been obtained by controlling the reduction rate of a polyol process. The products correspond to the morphology labeled A to E in Figure 1. The inset of (D) shows a typical electron-diffraction pattern of the branched nanostructures; F) enlarged section of the SEM image shown in (E) of the nanowires grown at the surface layer.

display a number of distinct morphologies depending on the experimental conditions. Figure 2 A shows a TEM image of the Pt nanoparticles when the reduction of the Pt^{II} intermediate was performed under nitrogen in the absence of an Fe^{II} or Fe^{III} species. The nanoparticles were roughly spherical in shape, with a mean diameter of about 5 nm. Note that the spherical shape is what we expect for a face-centered cubic metal formed under thermodynamic control.[16]

Figure 2 B shows a TEM image of the Pt nanoparticles that were obtained under conditions similar to those used in Figure 2 A, except that 50 μM Fe^{II} or Fe^{III} species had been added. In this case, the particles are larger and start to branch into a star shape. Figure 2 C shows a TEM image of a sample that was obtained by reducing the Pt^{II} intermediate in air for

10 h. Due to the presence of oxygen, the reduction was much slower (relative to the reaction that resulted in particles of Figure 2B) and the product became more highly branched and eventually entangled into large agglomerates. Figure 2D shows a TEM image of the product that was obtained when the Pt^{II} intermediate was heated in air for 10 h, followed by the introduction of nitrogen for 1 h. The resultant nanostructures branch out to generate multipods with a diameter of around 50 nm. The inset shows a typical electron diffraction pattern recorded from an ensemble of such highly branched nanostructures which confirms that they are composed of pure face-centered cubic Pt.

Figure 2E shows an SEM image of the Pt structures when the iron-mediated reduction was carried out in air. Similar to that seen in a previous study,[11] the final product contained micrometer-scale agglomerates of Pt nanoparticles with their surfaces covered by a dense array of uniform nanowires. These agglomerates could further fuse into larger structures. Figure 2F gives a magnified view of the portion indicated by a box in Figure 2E. It is clear that the as-synthesized nanowires were monodisperse in size distribution and their averaged diameter was around 5 nm. Because the nanowires were loosely attached to the surface of each agglomerate, they could be readily released by brief sonication without breaking the agglomerates. As we have demonstrated before, the released nanowires could be recovered by centrifugation and then dispersed in ethanol or water without introducing additional surfactants.[11]

Figure 3 A–C show TEM images of a Pt multipod that were recorded by tilting the sample at different angles relative to the electron beam. The arrow in Figure 3A indicates the axis against which the TEM grid was rotated by either −45° (Figure 3B) or +45° (Figure 3C). From the images, we conclude that this Pt nanostructure is a tetrapod, with four "arms" of roughly equal length. Figure 3D shows a typical high-resolution (HR)TEM image of the end of an arm that reveals its single-crystalline structure and the ⟨111⟩ growth direction for each arm. The lattice spacing between the [111] planes, 0.23 nm, is consistent with that of the bulk crystal. In the current stage of development, the final product of each synthesis is usually a mixture of multipods that contain between two to six arms. Some of these products were single crystals and others contained twin defects.

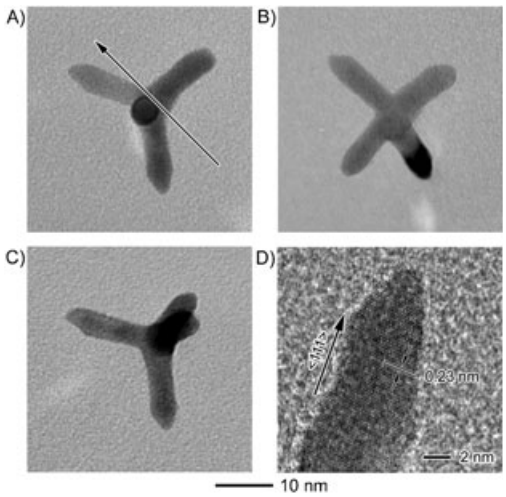

Figure 3. TEM images of a Pt tetrapod tilted at different angles to the axis indicated as an arrow: A) 0°, B) −45°, and C) 45°. The sample was taken from the product shown in Figure 1C. D) HRTEM image of one of the ends of this Pt tetrapod, which indicates that each arm was a single crystal with its growth direction along the ⟨111⟩ axis.

Figure 4 compares two types of four-armed nanostructures that we have observed: the first type is a tetrahedral configuration (Figure 4A) whereas the second has a square-planar structure (Figure 4C). Their HRTEM images (Figure 4B and 4D, respectively) clearly indicate that the tetrapod is a single crystal and the square-planar structure has a twin plane in the middle of the nanostructure. As a result of this structural difference, the angles between adjacent arms are also substantially different. For the tetrahedral configuration, we believe that there was only one single-crystal seed involved and the four arms simply grew out of different sites (four of the eight corners) of the seed.

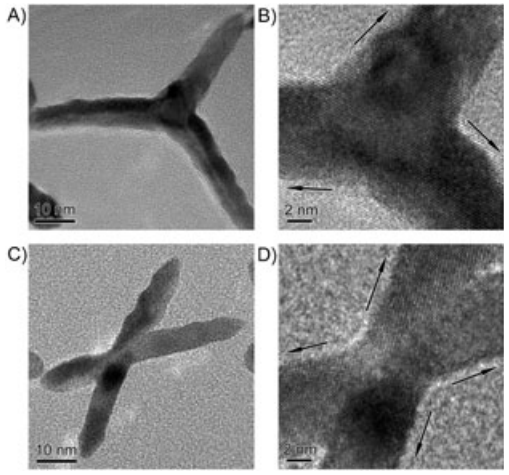

Figure 4. TEM and HRTEM images of two types of four-armed Pt nanostructures with different configurations: A), B) tetrahedral; C), D) square-planar. The HRTEM images indicate that all the arms grew along the ⟨111⟩ direction. While the square-planar structure has a twin plane in the middle, the tetrahedral structure is a single crystal because all four arms display the same fringe spacing and orientation.

In summary, we have demonstrated that Pt nanostructures with four different morphologies could be synthesized by controlling the reduction kinetics of a polyol process. The presence of both iron species and oxygen (or air) was found to be critical to the control of the reduction kinetics and hence morphology. Depending on the way the Fe^{II}/Fe^{III} redox pair and oxygen (from air) were supplied to the reaction system, Pt nanostructures in the form of spheres, star-shaped particles, branched multipods, and nanowires could be obtained as the major product for each run of synthesis. Although the strategy described here may resemble what has been widely explored in the general area of biomineralization,[17] the exact approaches are very different. In biomineralization, a biopolymer is used to mediate the diffusion rate of reactive species

toward the surface of nuclei and thus to control the morphology. In the approach presented here, the growth of nuclei is retarded by blocking their surface with oxygen and/or by facilitating the dissolution of atoms from the nuclei. The net results of these two different approaches are the same: a reduction in supersaturation and the induction of morphologies that deviate from those favored thermodynamically.[18]

Although the reduction kinetics could also be controlled by varying other experimental conditions such as temperature, it seems that the introduction of Fe^{II}/Fe^{II} redox species and oxygen was the most convenient and versatile variable. For instance, we have also performed the synthesis at 100, 80, and 50 °C. While the reduction became notably slower at both 100 and 80 °C, it was still too fast to generate Pt nanostructures other than spherical particles. At 50 °C, the reduction of Pt^{II} species ceased and no Pt^0 species were observed after several days. We expected that these results will open the door to a systematic study on the control of shape and thus properties associated with metal nanostructures.

Experimental Section

In a typical synthesis, ethylene glycol (EG, J. T. Baker; 4 mL) was placed in a three-neck flask equipped with a reflux condenser and a magnetic stirring bar embedded in PYREX glass and heated in air at 110 °C for 1 h to remove any trace water. Hexachloroplatinic acid (H_2PtCl_6, 0.033 g; Aldrich) and poly(vinyl pyrrolidone) (PVP, $\bar{M}_W$ = 55000, 0.045 g; Aldrich) were dissolved separately in ethylene glycol (2 mL) at room temperature. The molar ratio between H_2PtCl_6 and the repeating unit of PVP was controlled at 1:5. These two EG solutions were then added dropwise simultaneously to the reaction flask within 1.5 min. The reaction mixture was heated at 110 °C in air for 1.5 h. The solution turned from golden orange to green–yellow, indicating the formation of Pt^{II} species as the intermediate. The reaction mixture was then heated in a nitrogen atmosphere and turned brown and finally dark brown in 1 h. For iron-mediated synthesis, the iron species (20 μL of 20 mM of $FeCl_3$ or $FeCl_2$ predissolved in EG; Aldrich) was introduced into the system after the reaction had proceeded in air at 110 °C for 1.5 h (or when the solution turned green–yellow). The resulting solution was colorless and a black precipitate settled at the bottom of the flask. When a nitrogen atmosphere was present for different periods of time during the iron-mediated reduction, products with different morphologies were obtained: 1) starlike nanoparticles were formed when a nitrogen atmosphere was supplied immediately after the formation of Pt^{II} species; 2) branched nanostructures were produced when a nitrogen atmosphere was supplied after the Pt^{II} species had been left in air and at 110 °C for 10 h. In general, the longer the Pt^{II} species were kept in air before application of nitrogen, the more the final product would agglomerate. In the last step, the product was collected by centrifugation, washed with ethanol several times to remove ethylene glycol and excess PVP, and characterized by SEM, TEM, and HRTEM. The SEM images were taken by using a field emission microscope (FEI, Sirion XL) operated at an accelerating voltage of 10–20 kV. The TEM images and diffraction patterns were obtained with a JEOL microscope (1200EX II) operated at 80 kV. The HRTEM images were captured on a Tecnai G^2 F20 operated at 200 kV.

Received: November 19, 2004
Revised: January 22, 2005
Published online: March 17, 2005

Keywords: kinetic control · nanostructures · platinum · reduction

[1] a) R. Narayanan, M. A. El-Sayed, *J. Phys. Chem. B* **2004**, *108*, 5726; b) Z. L. Wang, T. S. Ahmad, M. A. El-Sayed, *Surf. Sci.* **1997**, *380*, 302; c) D. J. Milliron, S. M. Hughes, Y. Cui, L. Manna, J. Li, L.-W. Wang, A. P. Alivisatos, *Nature* **2004**, *430*, 190; d) X. Peng, L. Manna, W. Yang, J. Wickham, E. Scher, A. Kadavanich, A. P. Alivisatos, *Nature* **2000**, *404*, 59; e) S.-M. Lee, Y.-M. Jun, S.-N. Cho, J. Cheon, *J. Am. Chem. Soc.* **2002**, *124*, 615; f) F. Kim, S. Connor, H. Sond, T. Kuykendall, P. Yang, *Angew. Chem.* **2004**, *116*, 3759; F. Kim, S. Connor, H. Sond, T. Kuykendall, P. Yang, *Angew. Chem.* **2004**, *116*, 3759; *Angew. Chem. Int. Ed.* **2004**, *43*, 3673; g) T. K. Tapan, C. J. Murphy, *J. Am. Chem. Soc.* **2004**, *126*, 8648; h) S. Chen, Z. Wang, J. Ballato, S. H. Foulger, D. L. Carroll, *J. Am. Chem. Soc.* **2003**, *125*, 16186; i) M. Pileni, *Nat. Mater.* **2003**, *2*, 145.

[2] For example: F. A. Cotton, G. Wilkinson, *Advanced Inorganic Chemistry*, 5th ed., Wiley, New York, **1988**, pp. 868.

[3] a) A. Rouxoux, J. Schulz, H. Patin, *Chem. Rev.* **2002**, *102*, 3757; b) K. R. Williams, G. T. Burstein, *Catal. Today*, **1997**, *38*, 401.

[4] a) R. Narayanan, M. A. El-Sayed, *Nano Lett.* **2004**, *4*, 1343; b) L. M. Falicov, G. A. Somorjai, *Proc. Natl. Acad. Sci. USA* **1985**, *82*, 2207.

[5] a) T. Teranishi, M. Hosoe, T. Tanaka, M. Miyake, *J. Phys. Chem. B* **1999**, *103*, 3818; b) S. Chen, K. Kimra, *J. Phys. Chem. B* **2001**, *105*, 5397; c) H. Wakayama, N. Setoyama, Y. Fukushima, *Adv. Mater.* **2003**, *15*, 742; d) X. Teng, D. Black, N. J. Watkins, Y. Gao, H. Yang, *Nano Lett.* **2003**, *3*, 261.

[6] T. S. Ahmadi, Z. L. Wang, T. C. Green, A. Heglein, M. A. El-Sayed, *Science* **1996**, *272*, 1924.

[7] S. Zhao, S. Chen, S. Wang, D. Li, H. Ma, *Langmuir* **2002**, *18*, 3315.

[8] a) Y. Sakamoto, A. Fukuoka, T. Higuchi, N. Shimomura, S. Inagaki, M. Ichikawa, *J. Phys. Chem. B* **2004**, *108*, 853; b) A. Husain, J. Hone, H. W. C. Postma, X. M. H. Huang, T. Drake, M. Barbic, *Appl. Phys. Lett.* **2003**, *83*, 1240; c) X. Fu, Y. Wang, N. Wu, L. Gui, Y. Tang, *J. Mater. Chem.* **2003**, *13*, 1192; d) H. J. Shin, R. Ryoo, Z. Liu, O. Terasaki, *J. Am. Chem. Soc.* **2001**, *123*, 1246; e) Y. Han, J. Kim, G. D. Stucky, *Chem. Mater.* **2000**, *12*, 2068.

[9] a) B. Mayers, X. Jiang, D. Sunderland, B. Cattle, Y. Xia, *J. Am. Chem. Soc.* **2003**, *125*, 13364; b) Y. Sun, B. Wiley, Z.-Y. Li, Y. Xia, *J. Am. Chem. Soc.* **2004**, *126*, 9399.

[10] T. Kijima, T. Yoshimura, M. Uota, T. Ikeda, D. Fujikawa, S. Mouri, *Angew. Chem.* **2004**, *116*, 203; T. Kijima, T. Yoshimura, M. Uota, T. Ikeda, D. Fujikawa, S. Mouri, *Angew. Chem.* **2004**, *116*, 230; *Angew. Chem. Int. Ed.* **2004**, *43*, 228.

[11] J. Chen, T. Herricks, M. Geissler, Y. Xia, *J. Am. Chem. Soc.* **2004**, *126*, 10854.

[12] J. M. Petroski, Z. Wang, T. C. Green, M. A. El-Sayed, *J. Phys. Chem. B* **1998**, *102*, 3316.

[13] T. Mallat, A. Baiker, *Catal. Today* **1994**, *19*, 247.

[14] T. Herricks, J. Chen, Y. Xia, *Nano Lett.* **2004**, *4*, 2367.

[15] X. Peng, *Adv. Mater.* **2003**, *15*, 459.

[16] Z. L. Wang, *J. Phys. Chem. B* **2000**, *104*, 1153.

[17] S. Mann, *Biomineralization: Principles and Concepts in Bioinorganic Materials Chemistry*, Oxford University Press, **2001**.

[18] A. Chernov, *Phys. Crystallogr.* **1972**, *16*, 734.

